Propagation of electromagnetic ion cyclotron wave energy in the magnetosphere

T. M. Loto'aniu,[1] B. J. Fraser, and C. L. Waters

Cooperative Research Centre for Satellite System, Department of Physics, University of Newcastle, New South Wales, Australia

Received 1 October 2004; revised 5 January 2005; accepted 24 March 2005; published 15 July 2005.

[1] Recent satellite and conjugate observations of Pc 1 electromagnetic ion cyclotron (EMIC) waves have cast doubt on the validity of the long-standing bouncing wave packet (BWP) model that describes their propagation in the magnetosphere. A study was undertaken using the Combined Release and Radiation Effects Satellite (CRRES) E and B field data to further the understanding of the propagation characteristics of Pc 1 EMIC waves in the middle magnetosphere. CRRES covered the region L = 3.5–8.0, magnetic latitude up to ±30°, and magnetic local time 1400–0800. From 6464 hours of observation a total of 248 EMIC wave events were identified. For the first time the Poynting vector for Pc 1 EMIC waves is presented in the dynamic spectral domain permitting the study of energy propagation of simultaneous waves located in different frequency bands. The maximum wave energy flux for the events was 25 $\mu W/m^2$, averaging range 1.3 $\mu W/m^2$, with the direction of wave energy propagation independent of wave frequency but dependent on magnetic latitude. EMIC wave energy propagation was bidirectional both away and toward the equator, for events observed below 11° |MLat|. Unidirectional wave energy propagation away from the equator was observed for all events located above 11° |MLat|. This supports the concept of unidirectional EMIC wave energy propagation away from a broad source region centered on the geomagnetic equator. No measurable energy was observed propagating equatorward beyond the source region, in contradiction to the BWP paradigm.

Citation: Loto'aniu, T. M., B. J. Fraser, and C. L. Waters (2005), Propagation of electromagnetic ion cyclotron wave energy in the magnetosphere, *J. Geophys. Res.*, *110*, A07214, doi:10.1029/2004JA010816.

1. Introduction

[2] Early ground-based conjugate observations of pearl Pc 1 EMIC waves showed a wave structure that was band limited with an approximately 180° phase shift between wave packets observed in each hemisphere [e.g., *Tepley*, 1964]. This alternating pearl type structure between hemispheres was interpreted by *Jacobs and Watanabe* [1964] and *Obayashi* [1965] by the field-aligned Bouncing Wave Packet (BWP) model. An important parameter for establishing whether EMIC wave packets bounce according to the BWP model is the propagation direction of wave packet energy, the Poynting vector which requires both electric and magnetic wave field observations. Poynting vector measurements cannot be made from the ground observations and in situ observations of EMIC wave fields in the magnetosphere are required.

[3] Early spacecraft Poynting vector observations of EMIC wave energy were typically made using one component of the wave electric field along with the vector wave magnetic field, chosen to give the instantaneous field-aligned component of the Poynting vector. For example, *Mauk and McPherron* [1980] measured the electric field from $\vec{v} \times \delta\vec{B}$ plasma drift, while *Erlandson et al.* [1990, 1992] used Viking data at midaltitudes and high latitudes (L = 3.8–19). The *Erlandson et al.* [1990] study derived field-aligned Poynting vectors for 21 EMIC wave events (f = 0.1–3.0 Hz) and found field-aligned wave energy (~10–100 $\mu W/m^2$) predominately propagated toward the ionosphere. In the *Erlandson et al.* [1992] study a series of EMIC wave bursts ($f \approx$ 1.5 Hz) occurring about 67 s apart were observed and wave packet field-aligned energy flux was again found to be directed downward into the ionosphere with a maximum reflection coefficient estimated ~0.1–0.2. They also found equatorially directed waves but concluded that these waves were not associated with the downward traveling wave packets. Partial Poynting vector estimates were also reported by *LaBelle and Treumann* [1992] of an EMIC wave event near the equator observed on the AMPTE/IRM satellite. Only one component of the δE field was available with field-aligned Poynting (~1 $\mu W/m^2$) showing the wave energy directed away from the equator. The Viking and AMPTE/IRM satellite results agree with the previous ATS 6 observations of *Mauk and McPherron* [1980]. These early observations, although unreliable, did introduce the

[1] Now at the Department of Physics, University of Alberta, Edmonton, Alberta, Canada.

0148-0227/05/2004JA010816$09.00

possibility of unidirectional EMIC wave propagation and the need for full Poynting vector measurements.

[4] *Fraser et al.* [1992] measured a Pc 2 EMIC wave event observed using wave field data from the ISEE 1-2 satellites. Taking the δE and δB wave fields that were perpendicular during a satellite spin cycle, they estimated the energy flux at 0.1 $\mu W/m^2$ and found the wave energy was predominately field-aligned. However, the small energy flux magnitude suggested that this value may be close to the ISEE instrumentation noise level and therefore unreliable. *Fraser et al.* [1996] used CRRES data to estimate the EMIC wave Poynting vector. Two components of the wave electric field and three components of the wave magnetic field were available, while the third electric field component was estimated by assuming plane wave propagation. They studied nine EMIC wave events observed by CRRES within $\pm 20^\circ$ MLat and over $L = 4.8-6.7$ and found average energy flux in the range $4-18$ $\mu W/m^2$. In eight of the nine cases, energy propagation was predominately away from the equator. The reflection coefficients were below 0.2, in agreement with the findings of *Erlandson et al.* [1992]. There were two events observed at $\leq 3^\circ$ |MLat|, which showed occasional bursts of EMIC wave energy toward the equator. They suggested that in these cases CRRES was most likely within the generation region.

[5] More recently, *Mursula et al.* [2001] observed a structured EMIC wave event on the Polar satellite, which was in good conjunction with Finnish ground stations. This was the first study of EMIC waves where all three measured components of δE and δB fields were available allowing full Poynting vector estimates. Polar observed the waves as two simultaneous EMIC wave events around the plasmapause at $16^\circ-30^\circ$ MLat and over $L = 4.3-6.2$. The Polar observations of the events with frequencies above the He+ cyclotron frequency f_{He+}, extended over a large latitudinal range of more than 5° and were seen on the ground as broad diffuse Pc 1 EMIC wave pearls. However, the magnetic field measurements of the waves with $f > f_{He+}$ were weak and no Poynting vector estimates were calculated. The Polar observations of the EMIC waves with frequencies below the local f_{He+} showed repetitive wave bursts and were observed on the ground as classical Pc 1 pearls. All three components of the Poynting vector in the He+ wave band were calculated. The field-aligned Poynting vector component, S_z, dominated and was positive ($\sim 20-25$ $\mu W/m^2$) with the wave energy propagating predominately away from the equator.

[6] Previous estimations of the EMIC wave Poynting vector have confined the calculation of energy flux to the time domain and no frequency dependence was considered. This limited the ability to study heavy ion and other frequency-dependent effects. Here the first estimates of the Poynting flux in the frequency domain are presented, providing a more complete frequency dependent understanding of wave energy flux propagation, including heavy ions effects. Two typical individual event case studies and some summary statistics are included to illustrate the characteristics of the overall data set.

2. Instrumentation and Data Analysis

[7] The Combined Release and Radiation Effects Satellite (CRRES) was launched in July 1990 into a low-inclination geosynchronous transfer elliptical orbit [*Singer et al.*, 1992; *Wygant et al.*, 1992; *R. R. Anderson et al.*, 1992]. The initial orbit period was about 10 hours, perigee was ~ 350 km and apogee ~ 6.3 R_E while orbit inclination was 18.2° and spin rate 2 rpm (~ 32 mHz). Apogee at launch was 0800 MLT and decreased in local time at a rate of 1.3 hours per month reaching 1400 MLT when the spacecraft ceased operation in October 1991. During normal onboard spacecraft operations, CRRES instruments observed the middle magnetosphere over $L = 3-8$ and up to $\sim 30^\circ$ |MLat| while the CRRES observations did not include 0800–1400 MLT unless the spacecraft was off the equator.

[8] The Air Force Geophysics Laboratory (AGFL) fluxgate magnetometer provided three components of the vector magnetic field from DC–8 Hz Nyquist. The University of California, Berkeley electric field/Langmuir Probes (EF/LP), which when operated in the electric field mode used two pairs of orthogonal sensors with tip-to-tip separations of 100 m, provided two components of the wave electric field sampled at 32 Hz. The University of Iowa/AFGL Plasma Waves Experiment (PWE) was used to estimate cold electron plasma densities at the CRRES locations through observations of the upper hybrid resonance frequency (f_{UHR}) [*R. R. Anderson et al.*, 1992].

[9] The measured fields were the wave electric fields δE_y and δE_z, and the total magnetic fields B_x, B_y and B_z all in MGSE coordinates, which is a modified version of the Geocentric Solar Ecliptic (GSE) system [e.g., *Kivelson and Russell*, 1996] where the X axis is allowed to move up to 15° off the Earth-Sun line. For compatibility with the magnetic field data the electric field data were resampled to 16 Hz. The total magnetic fields components were high pass filtered through a forward and reverse second-order Butterworth filter with a 0.1 Hz cutoff to extract the wave magnetic fields δB_x, δB_y, and δB_z. All the measured fields were then field-aligned so that the z-component was along the ambient magnetic field direction.

2.1. The δE_x Component Estimates

[10] In order to estimate the δE_x electric field component in field-aligned coordinates, electromagnetic plane wave propagation was assumed, which given the $\delta\vec{E}$ and $\delta\vec{B}$ field vectors satisfy

$$\delta\vec{E} \cdot \delta\vec{B} = 0. \tag{1}$$

Applying this dot product and rearranging to make δE_x the subject gives

$$\delta E_x = -\left[\frac{\delta B_y}{\delta B_x}\delta E_y + \frac{\delta B_z}{\delta B_x}\delta E_z\right]. \tag{2}$$

The calculation of δE_x using equation (2) has previously been considered by *Fraser et al.* [1996] using the CRRES data set and by *Fraser et al.* [1992] using data from ISEE-1. The top part of Figure 1 shows an example of the δE_x component estimated using equation (2). Inaccuracies in the measured electric field components can result in significant uncertainties in the estimates of δE_x. Errors introduced are of the order $|\delta B_y/\delta B_x|$ times the error in δE_y and likewise for δE_z. If the denominator, δB_x, is small the errors in δE_x can be very large. Therefore δE_x was estimated only when the

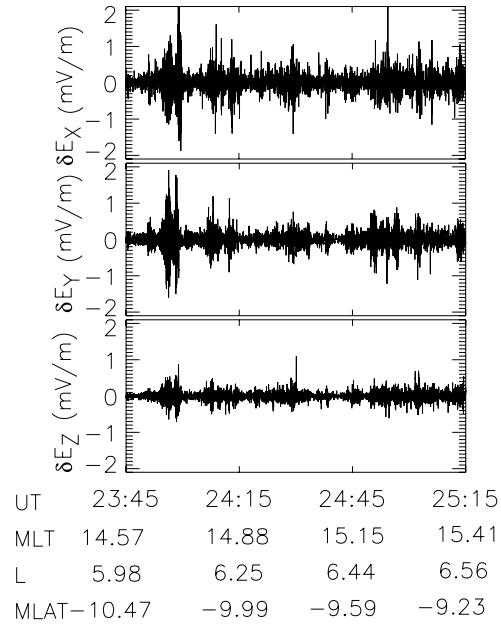

Figure 1. An example electric vector field time series in field-aligned coordinates taken from an EMIC event in orbit 962 of CRRES. The EMIC wave packets are clearly visible. The δE_y and δE_z components were measured by the CRRES EF/LP experiment, while δE_x calculated assuming plane wave propagation (see text).

magnetic field ratios were less than 5.5. This corresponds to the angle, β, between the CRRES spin plane and the total magnetic field vector having a value greater than 20° or the angle, α, between the spin axis and the total magnetic field vector less than 70°.

2.2. Magnetic and Electric Field Noise Estimates

[11] The EMIC wave events were identified by placing a threshold on the wave spectral power density (SPD). The signal to noise ratios were estimated by plotting the magnetic and electric field amplitude spectrograms for each wave event. Noise levels were found to be frequency dependent but varied slowly with frequency. Figure 2 shows an example of the δB_x component noise estimate for an event in CRRES orbit 962. The average wave frequency of all events in the current study was 0.71 Hz which corresponded to an average noise level over all EMIC wave events of less than 0.06 nT^2/Hz in power or less than ± 0.12 nT/$\sqrt{Hz}$ in amplitude. The error in magnetic field amplitude was set at ± 0.12 nT/$\sqrt{Hz}$ with the corresponding magnetic power threshold ~ 0.06 nT^2/Hz.

[12] Similarly, for the electric field data, the measured components, δE_y and δE_z electric power threshold was set at 0.03 $(mV/m)^2$/Hz with the error in amplitude ± 0.08 mV/m/$\sqrt{Hz}$. For the δE_x component the noise level was considerably higher than the measured components. In this case the electric power threshold was set at 0.09 $(mV/m)^2$/Hz with the error in amplitude ± 0.15 mV/m/$\sqrt{Hz}$.

2.3. Poynting Vector

[13] The primary aim of this study was to estimate the direction and magnitude of the EMIC wave Poynting flux in the spectral domain. In a homogeneous, isotropic, linear, and stationary medium the integral form of the Poynting theorem [e.g., *Lorrain et al.*, 1988] is given as

$$-\int_A \left(\delta\vec{E}\times\delta\vec{H}\right)\cdot d\vec{A} = \frac{d}{dt}\int_v \left(\frac{\epsilon\delta E^2}{2}+\frac{\mu\delta H^2}{2}\right)dv + \int_v \vec{J}_f\cdot\delta\vec{E}dv, \tag{3}$$

where $\delta B = \mu\delta H$ and where μ and ϵ are the magnetic permeability and the electric permittivity of the medium, respectively. The first integral on the right side of equation (3) gives the rate of increase of electromagnetic energy density inside a volume, v. The second term gives the rate at which part of the field energy dissipates as heat where J_f is the plasma current. For a plane wave in free space the absorption (lossy medium) term would be absent with $\vec{J}_f\cdot\delta\vec{E} = 0$. On the left side, the integral represents the rate at which electromagnetic energy flows into (negative sign) the volume and the part in brackets gives the Poynting vector

$$\vec{S} = \frac{1}{\mu}\left(\delta\vec{E}\times\delta\vec{B}\right) \tag{4}$$

and represents the electromagnetic energy flux through an area $d\vec{A}$. Since $\vec{S}$ is a vector, its direction gives the direction of energy propagation of the electromagnetic wave. For a plane wave traveling in a homogeneous, isotropic medium, equation (1) holds and the propagation direction coincides with the wave normal direction given by the wave vector, $\vec{k}$, and the group ray vector direction [e.g., *Walker*, 1993].

[14] However, the magnetospheric environment is inhomogeneous and the question arises as to the meaning of $\vec{S}$ in

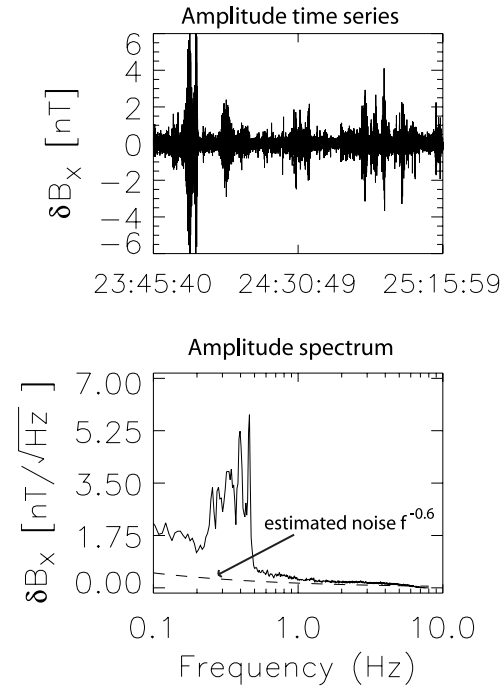

Figure 2. An example output of the noise level estimation for the δB_x wave magnetic field component in field-aligned coordinates. The noise function was proportional to $f^{-0.6}$ nT/$\sqrt{Hz}$. Power in the noise was less than 0.06 nT^2/Hz or less than ± 0.12 nT/$\sqrt{Hz}$ in amplitude over the event interval.

such a medium. Given wave fields and associated current densities that vary proportional to $\exp[i(\vec{k}\cdot\vec{r}-i\omega t)]$, the inhomogeneous medium after Fourier analysis can be described by the dielectric tensor $\epsilon(\omega, \vec{k})$ [e.g., *Stix*, 1992]. If space and time variations remain adiabatic, the medium can still be entirely characterized by the $\epsilon(\vec{r}, t, \omega, \vec{k})$, as long as the space and time variations occur at rates which are slow compared with the first-order variations in the electromagnetic fields.

[15] Consider a wave packet propagating with $\vec{k}$ and ω local quantities that vary adiabatically and the location of the wave packet given in space and time by $\vec{r}$ and t. The wave packet can be viewed as a superposition of plane waves which are spatially limited and $\vec{r}$ gives the point of maximum constructive interference at time t when the wave packet is centered on ω and $\vec{k}$ [e.g., *Stix*, 1992; *Walker*, 1993]. Using first-order quantities, the wave packet electric field can be represented by $\delta\vec{E} = Re[\delta\vec{E}_1\exp(-i\phi)]$, where the phase ϕ varies with $\vec{r}$ and t. The parameters $\vec{k}$ and ω may have small imaginary parts from $\phi = \phi_r + i\phi_i$ giving $\vec{k}_i = -\nabla\phi_i(\vec{r}, t)$ and $\omega_i = \partial/\partial t\phi_i(\vec{r}, t)$. Taking the time-averaged quantities in the Poynting theorem [e.g., *Walker*, 1993] over several cycles of the wave period, any terms in equation (3) which vary with the form $\exp(\pm i\phi_r)$ or $\exp(-2i\phi)$ will average to zero and only terms which vary according to $\exp(2\phi_i)$ are nonzero. Given two complex vectors $\vec{A}$ and $\vec{B}$, there are at least four terms in any of the products, which means that the averaged products must now be multiplied by one quarter. The zero-averaged terms in the products would be $\vec{A}\ \vec{B}$ and $\vec{A}^*\vec{B}^*$. For the dielectric tensor it is possible to split ϵ into its lossless, ϵ_h and lossy, ϵ_a, parts [e.g., *Stix*, 1992].

[16] Using the above assumptions and conditions, the time-averaged Poynting theorem may be expressed in differential form as

$$\nabla\cdot\vec{S}+\frac{\partial W}{\partial t}=-2\vec{k}_i\cdot\left(\vec{S}+\vec{T}\right)+2\omega_i W+\frac{\partial W}{\partial t_{\text{lossy}}}=0, \tag{5}$$

where

$$W=-\frac{1}{4}\left(\frac{\epsilon}{\mu}\right)^{1/2}\left[\delta\vec{B}^*\cdot\delta\vec{B}+\delta\vec{E}^*\cdot\frac{\partial}{\partial\omega}\left(\omega\vec{\epsilon}_h\cdot\delta\vec{E}\right)\right] \tag{6}$$

$$\frac{\partial W}{\partial t_{\text{lossy}}}=-\frac{\omega_r}{2}\left(\frac{\epsilon}{\mu}\right)^{1/2}\delta\vec{E}^*\cdot\epsilon_a\cdot\delta\vec{E} \tag{7}$$

$$\vec{T}=-\frac{\omega}{4}\left(\frac{\epsilon}{\mu}\right)^{1/2}\delta\vec{E}^*\cdot\frac{\partial}{\partial\vec{k}}\epsilon_h\cdot\delta\vec{E} \tag{8}$$

$$\vec{S}_{av}=\frac{1}{4\mu}\left(\delta\vec{E}^*\times\delta\vec{B}+\delta\vec{E}\times\delta\vec{B}^*\right). \tag{9}$$

The expression $\vec{T}$ is the flux due to nonelectromagnetic or acoustic energy resulting from coherent motion of the plasma, which is zero if a cold plasma is assumed (no acoustic flux) [e.g., *Allis et al.*, 1963]. The lossy term represents the rate of energy absorption by the dielectric medium. In equation (6) the first term on the right is the magnetic energy density and the second term is the sum of electrostatic and acoustic energy that comes from particle kinetic energy associated with coherent wave motion. The time-averaged Poynting vector, equation (9), defines the complex spectral Poynting vector density matrix in Fourier space. Allowing for complex wave fields and time averaging, this density matrix reduces to equation (4) for a homogeneous medium. Therefore even allowing for adiabatic variations in the medium properties, $\vec{S}$ still represents the flux of electromagnetic energy.

[17] It is noted that in an anisotropic medium, such as the magnetosphere, the wave normal and Poynting vector directions are not necessarily parallel. Assuming wave packets resulting from superposition of the plane waves, an immediate result would be that each wave has a slightly different frequency both in time and space due to the inhomogeneous medium. This dispersion results in the wave group velocity, V_g, differing from the phase velocity, V_p. The angle between V_g and the background magnetic field, B_o, is the group ray angle (ψ) while θ is the wave normal angle. For an inhomogeneous medium, ψ and θ may differ. However, independent of the medium the angle ψ coincides with the Poynting vector direction, as long as the group velocity vector describes the envelope of the wave packet and within that envelope constant phasing exist between individual waves [e.g., *Walker*, 1993].

[18] All six magnetic and electric wave field components in field-aligned coordinates were Fast Fourier transformed (FFT) and the density matrix represented by equation (9) calculated. The real components of this matrix are the spectral Poynting flux values. The implementation of the FFT and smoothing processes reduced estimates of the wave energy flux. A sine wave sampled at 16 Hz with amplitude of 1.0 was generated to determine an optimum Poynting vector multiplication factor. The number of points in the times series was 20,000 or at 16 Hz about 21 min, which was typical of times series lengths analyzed in this study. The frequency of this test wave was 0.71 Hz, which is the average frequency of the EMIC wave events analyzed. The multiplication factor to calibrate the spectral Poynting flux was determined to be 7.1. This multiplication factor was also confirmed by estimating the time domain energy flux for three long time duration EMIC wave events and comparing the values to the spectral domain values for the same events. The restoration of the spectral energy flux level allows direct comparison between the time and frequency domain representation of the Poynting vector.

[19] Since EMIC waves propagate essentially parallel to the ambient magnetic field the field-aligned Poynting vector component, S_z, is the important component and is the component shown in this paper. Uncertainty in the Poynting vector values were estimated using the errors in the δE and δB fields (section 2.2) and were found to be less than 0.1 μ W/m^2/Hz for the S_z component. Other dynamic spectrograms produced were of EMIC wave cross power and wave ellipticity. Typical spectrogram parameters were an FFT length of 800 points (50 s) with a step time of 150 points (9.4 s) giving a frequency resolution of 0.02 Hz.

3. Results

[20] In total 6464 hours of CRRES observation covering about 10 months in the period 7 September 1990 to 9 October 1991 were searched for EMIC waves. The period from 15 October 1990 to 9 January 1991 were not suitable

for EMIC wave Poynting vector studies because either the simultaneous magnetic and electric field data were not available or one or more of the instruments of interest were not operational. An EMIC wave event was identified if its wave electric and magnetic field power was above thresholds determined from the signal to noise ratios (section 2.2) for at least 60 s in both the magnetic or electric spectrograms. There were 248 EMIC wave events identified, with 144 and 104 events observed below and above the local f_{He+}, respectively. Event frequencies ranged from 0.1 to 3.1 Hz and were seen at latitudes up to ~26° |MLat|. Most events were seen at higher L values near apogee where CRRES spends the majority of its time while the wave occurrence over MLT peaked in the late afternoon [e.g., *Fraser and Nguyen*, 2001].

3.1. Wave Event Located at |MLat| > 11°

[21] The middle part of Figure 3a shows the wave transverse magnetic cross power density spectrogram for an event observed by CRRES during orbit 923 on 11 August 1991 between 0620 and 0707 UT (15.4–15.9 MLT), MLat ≈ −24°, and L = 7.3–7.6, in the afternoon. The two black lines running across each part are the local He+ (f_{He+}) and O+ (f_{O+}) cyclotron frequencies. Over the event interval, CRRES was moving outbound through the plasma trough and near apogee while the electron density deduced from the f_{UHR} (not shown), varied between 13 and 18 cm^{-3} and the Alfvén velocity, V_a, 1000–800 km/s. The *Dst* average during the event was +35 nT and the average Kp value was 4. The PWE spectrogram (not shown) revealed a sharp density gradient at $L \sim 3.9$, indicating the plasmapause location.

[22] The top part of the figure shows S_z, the parallel component of the Poynting flux, in field-aligned coordinates and EMIC wave bursts are seen both above and below the local f_{He+}. In this event the EMIC waves of interest are restricted to those above f_{O+}. Wave frequency ranges from f = 0.81–1.32 Hz ($f/f_{H+} = X_{\mathrm{local}}$ = 0.38–0.52, $f/f_{H+} = X_{eq}$ = 0.77–1.1) for the events above f_{He+} and f = 0.42–0.61 Hz (X_{local} = 0.18–0.24, X_{eq} = 0.39–0.49) for those below f_{He+}. The color bar indicates the magnitude of the flux with yellow to red positive (south to north or toward the equator) energy flux and light blue to dark-blue negative (north to south or away from the equator) energy flux. Ranging from −1.3 to −10.0 μW/m^2/Hz, the S_Z component was on average four times larger than the transverse components (not plotted) and showed unidirectional energy flux moving toward the Southern Hemisphere and away from the equator for all wave packets, independent of wave packet frequency. The dynamic spectral wave ellipticity spectrogram is shown in the bottom part. Most of the wave packets show linear-LH polarized, as expected for EMIC waves [*B. J. Anderson et al.*, 1992].

3.2. Wave Event Located at |MLat| < 11°

[23] On 8 May 1991, CRRES observed an event shown in Figure 3b during a magnetically moderate day, between 1800 and 1815 UT (18.84–19.09 MLT), while it was outbound at |MLat| ≈ 10.5° and $L \sim 6.0$. During the event average, *Kp* was 3, while *Dst* was +1 nT. The plasmapause was not well defined for this day with the edge of the plasmasphere reaching $L \sim 6.0$. Electron density (not shown) decreased from 80 cm^{-3} to 40 cm^{-3} during the event while the Alfvén velocity (not shown) was constant and low at 550 km/s. The cross power spectrogram (second part of Figure 3b) shows the event occurred predominately below f_{He+} with f = 0.27–0.32 Hz (X_{local} = 0.11–0.13, X_{eq} = 0.14–0.56). However, there were also wave packets above f_{He+} but in this case only the central wave packet, *i*, at 1803 UT where f = 0.66 Hz (X_{local} = 0.26, X_{eq} = 0.31) was considered part of the event for this study. The field-aligned Poynting vector (top) shows bidirectional wave energy propagation, both toward and away from the equator with flux ranging from 2.5 to −8.0 μW/m^2/*Hz*. Each energy packet is labeled, and in particular energy packets with $f < f_{He+}$ ($a - h$) show pearl structure with alternating propagation directions ($b - h$). Wave packet *i* propagates away from the equator the same as *a* which is coincident in time. The dynamic spectral wave ellipticity spectrogram is shown in the last part where the wave packets are mostly linearly polarized.

3.3. Wave Energy Flux and Magnetic Latitude Dependence

[24] The variation in EMIC wave S_z flux with latitude |MLat| for all 248 EMIC events are shown in Figure 4 and Table 1 summarizes the statistical results. The error in Poynting vector magnitude (see section 2.3) is below the visible resolution in the figure. The dotted vertical lines indicate the ±11° MLat locations. Combining both hemispheres, wave energy flux magnitude ($|S_z|$) was maximum at |MLat| = 7° with $|S_z|$ = 25 μW/m^2, while the average over all events was 1.3 μW/m^2. Of the 248 events, 33% (81) occurred above 11° |MLat|, and from these all showed unidirectional S_z propagating away from the equatorial region. Below 11° |MLat| bidirectional energy flux propagation was seen for 26% (44) of the 167 events in this region. An event was considered bidirectional if it had at least two wave packets in the S_z component with fluxes in opposing directions and above 0.1 μW/m^2/Hz continuously for at least 60 s.

4. Discussion

4.1. Wave Event Located at |MLat| > 11°

[25] The first event observed on 11 August at 0620–0707 UT and presented in section 3.1 occurred in the low-density plasma trough region. The event was not associated with plasma enhancement in the plasma trough. Simultaneous wave power seen in the He+ and H+ wave branches (Figure 3a) and the existence of two spectral gaps which followed the local cyclotron frequencies f_{He+} and f_{O+}, suggest that both He+ and O+ ions were present in the plasma trough during the event [*Fraser*, 1985]. The field-aligned energy flux (S_z) results (top part of Figure 3a) shows the advantage of estimating the wave energy flux in the frequency domain. Energy propagation of EMIC wave packets, which have different frequencies or harmonic structure, can be identified. The unidirectional energy propagating away from the equatorial region was independent of event frequency or wave branch, suggesting that both the He+ and H+ wave branches do not undergo BWP propagation. Propagation away from the equator suggests

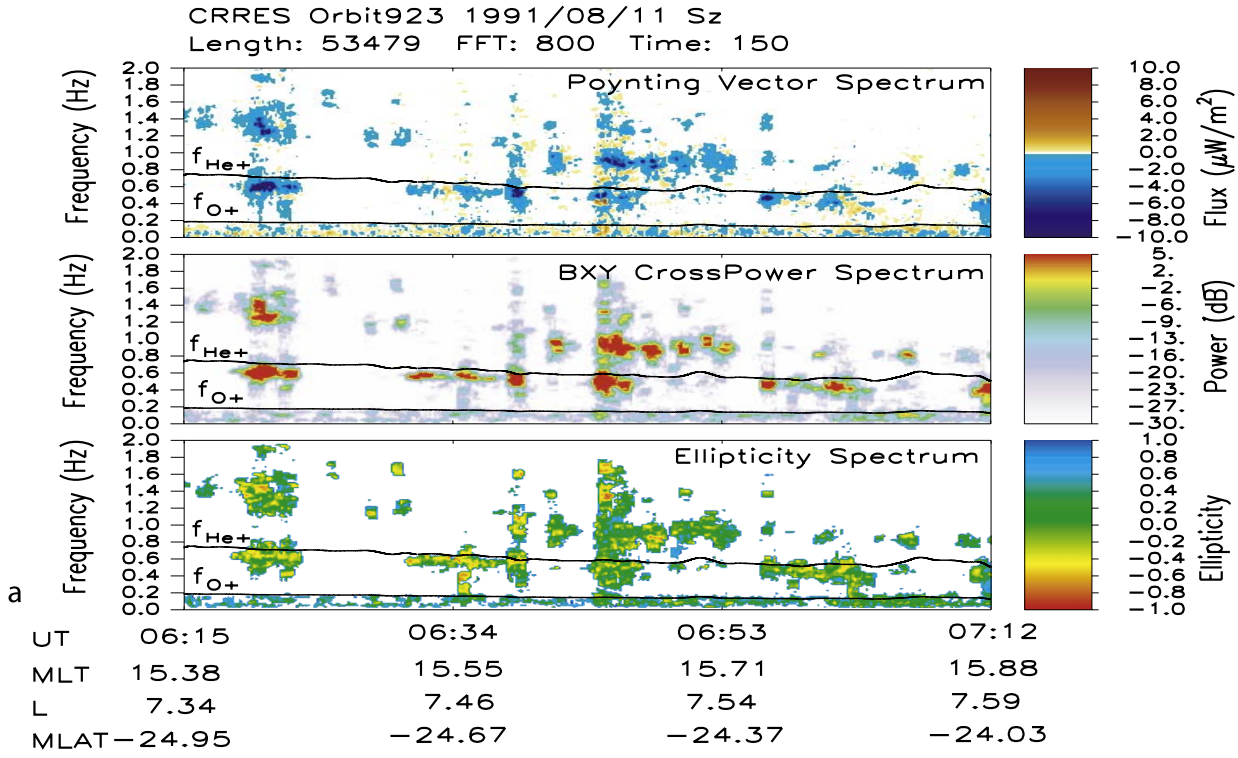

a

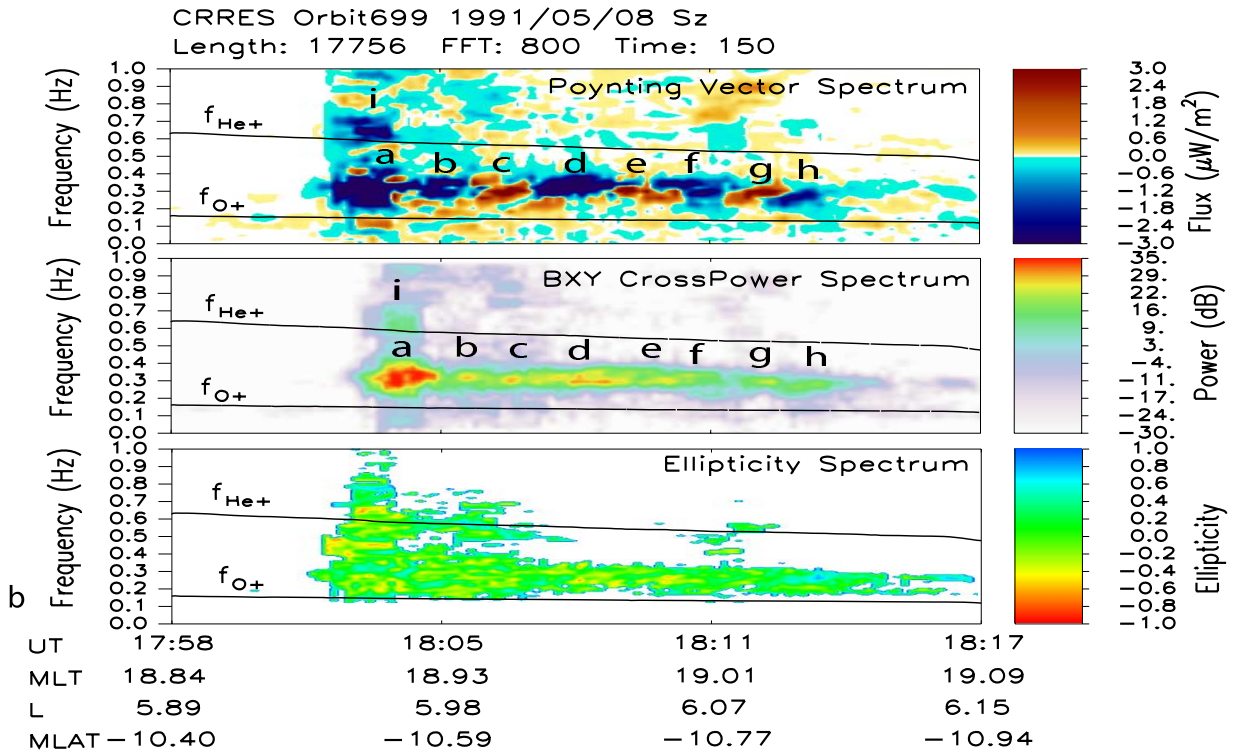

b

Figure 3. (a) The 11 August 1991 0620–0707 UT EMIC wave event showing the field-aligned Poynting vector (S_z), magnetic cross power, and wave ellipticity spectrograms. The data-sampling frequency was 16 Hz, while the dynamic spectrograms were produced with an FFT of 800 points and a slide time of 150 points. (b) An EMIC wave event observed by CRRES on 8 May 1991. The spectrograms shown are of the field-aligned Poynting vector (S_z), magnetic cross power, and wave ellipticity. The data-sampling frequency was 16 Hz, while the dynamic spectrograms were produced with an FFT of 800 points and a slide time of 150 points.

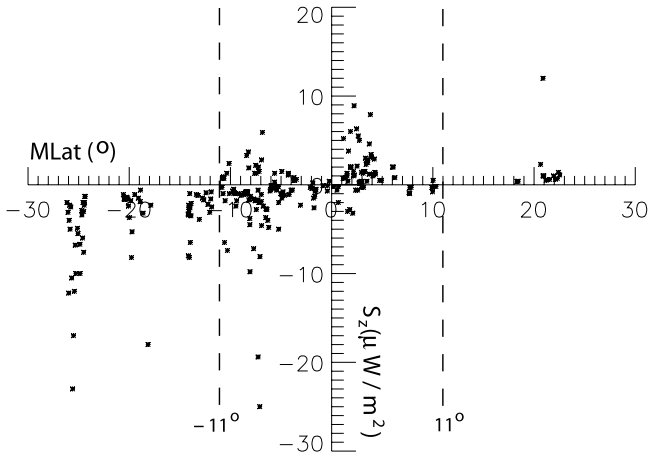

Figure 4. EMIC wave field-aligned Poynting vector (S_z) versus MLat for all 248 events for both hemispheres combined. Errors in S_z are below the visible resolution. The dotted vertical lines indicate the ±11° MLat locations. Table 1 summarizes the statistical results from this figure.

that the EMIC waves were generated near the equator and propagated into higher magnetic field regions, consistent with earlier studies [e.g., *Kaye and Kivelson*, 1979; *Fraser and Nguyen*, 2001; *Mursula et al.*, 2001].

[26] However, when the event wave frequencies were normalized to the equator, the higher wave band shows some wave energy with $X_{eq} > 1.0$ and for the lower band all the wave energy were observed at $X_{eq} > 0.25$. This would suggest that this event was generated off the equator close to the observation site. In section 4.3 the statistics for all events are discussed and it is shown (see Figure 4) that bidirectional EMIC wave energy flux is observed up to 11° off the magnetic equator. This would suggest that the 11 August EMIC wave event was generated up to 11° off the magnetic equator and then propagated to higher latitudes where it was observed by CRRES at |MLat| ~24°. The event also occurred when the dayside magnetosphere was in extreme compression, as suggested by the +35 nT *Dst* index. Under such conditions, the equatorial magnetic field is intensified leading to excessively large calculated normalized frequencies, which may explain the large normalized frequencies seen for this event. Also, the field lines may be greatly distorted at the dayside and the minimum field intensity region, and thus the EMIC growth region may shift from the equator to a larger MLat. The bursty structure in the event is due also to the fact that the event occurred during a magnetically active period.

[27] The EMIC wave event was observed at |MLat| ~ 24° and $L \sim 7.5$, which is beyond the H+ branch bi-ion (f_{bi}) and crossover (f_{xo}) frequency locations which were estimated at |MLat| ~ 15°–20°. The f_{bi} and f_{xo} locations were calculated assuming a dipole field configuration and H+-He+ ion plasma with 7% He+ ions. If the event was generated in the equatorial source region the wave power and energy at |*MLat*| ~24° does not seem to have been affected by the f_{xo} and f_{bi}, which does not agree with accepted theoretical studies [e.g., *Young et al.*, 1981; *Perraut*, 1982; *Rauch and Roux*, 1982; *Perraut et al.*, 1984; *Fraser*, 1985]. The spectral gap, however, does suggest a nonpropagation stop band between the cutoff frequency (f_{co}) and the ion cyclotron frequency locations. According to *Rauch and Roux* [1982], the H+ wave branch should encounter a polarization reversal at the off equatorial f_{xo} location while the He+ wave branch should not be affected by this f_{xo} location assuming the absence of O+ ions. However, the ellipticity results show no meaningful difference between the two wave branches and the amount of linear polarization in the H+ frequency branch waves (bottom part of Figure 3a) suggests that polarization reversal due to the crossover frequency was not significant. If parallel propagation is assumed, the H+ branch waves would not be affected by the f_{xo} and f_{bi} locations and the wave energy could reach the ionosphere where some of this energy may be reflected. However, the results show no significant energy propagation toward the equator. Furthermore, the He+ wave branch should also be reflected at the ionosphere according to the BWP paradigm, but no significant energy is seen propagating toward the equator in this wave branch.

4.2. Wave Event Located at |MLat| < 11°

[28] The 8 May event (section 3.2) occurred at |MLat| < 11°, predominately in the He+ wave band, and showed bidirectional wave energy propagation (top part of Figure 3b), suggesting it may have been observed within the equatorial generation region. The wave Alfvén velocity was low at 550 km/s while for the 11 August event (section 3.1), which occurred well off the equator (~24° |MLat|), V_a was nearly twice as high as this. Within the equatorial generation region the relatively low ambient magnetic field (B_o) and V_a results in a minimum resonant energy (E_R) favoring wave generation [e.g., *Criswell*, 1969; *Gendrin*, 1975; *Kaye et al.*, 1979]. The cross power (B_{xy}) spectrogram (middle part of Figure 3b) was saturated at 5 dB but when uncapped showed repetitive wave packet structure in the He+ wave branch. The repetitive energy packets observed in S_z suggests that the event was a structured or "pearl" EMIC wave with the bidirectional energy flux for wave packets *b* to *h* predicted by the BWP model. According to the BWP model, the "pearl" structure observed in S_z occurs because some of the wave energy of the EMIC waves, generated in the equatorial region of the magnetosphere and propagating away from the equator, is reflected and bounces back and forth along the geomagnetic field line between ionospheric mirror points [*Jacobs and Watanabe*, 1964; *Obayashi*, 1965].

[29] The theoretical travel times for the wave packets to travel to the ionosphere and back to the CRRES location were calculated using the T87 magnetic field model [*Tsyganenko*, 1987], assuming MLat = −10°, $L = 6.0$, and a plasma density of 50 e$^-$/cm^3. For propagation to the northern hemisphere and back to CRRES, $\tau_n \sim 140$ s, while for the southern hemisphere, $\tau_s \sim 80$ s with $\tau_n > \tau_s$ expected since CRRES was located below the equator. This gives a

Table 1. A Summary of the Field-Aligned EMIC Wave Poynting Vector (S_z) Statistical Results

Events	>11° |MLat|	<11° |MLat|
Total	33% (81)	67% (167)
Bidirectional	0% (0)	26% (44)
Unidirectional	100% (81)	74% (123)

total bounce period of ≈220 s. The mean observed repetition time between wave packets was 90 ± 16 s, independent of the direction of wave propagation. The error was taken as the largest difference between the average and each repetition time. The magnetic latitude of CRRES were estimated using the Olson-Pfitzer 1977 magnetic field model [*Olson and Pfitzer*, 1974]. It could be that the actual magnetic latitude of CRRES was much closer to the equator, which would give $\tau_n \sim \tau_s$. However, it has been shown that at L = 6.0 there is no significant difference between the Olson-Pfitzer and more realistic models such as the T87 model [e.g., *Loto'aniu et al.*, 1999].

[30] The experimental average double-hop bounce period of ≈180 s is close to the theoretical total bounce value of ≈220 s predicted by the BWP model. However, the fact that the statistical result in Figure 4 shows that CRRES observes no equatorially directed wave energy above 11° |MLat| would suggest that any observed periodic wave packet structure is not due to bouncing wave packets. It is suggested that the event is located within the equatorial generation region and that the bidirectional energy flux may be a generation effect, although the reason for the energy packet periodicity is unknown. It could result from Pc 5 modulation of the EMIC waves [e.g., *Mursula et al.*, 1997, 2001]. On average, however, simultaneous compressional Pc 5 wave amplitudes were less than 0.3 nT over the Pc 1 EMIC wave event. *Gail* [1990] has shown that positive wave growth rates can occur for equilibrium anisotropy which is less than the critical anisotropy, but further theoretical studies are required to fully understand this mechanism within the generation region.

4.3. Statistics

[31] The distribution of the 248 EMIC events over L value, |MLat|, and MLT agrees with previous in situ studies of EMIC waves in the middle magnetosphere [e.g., *Bossen et al.*, 1976; *Mauk and McPherron*, 1980; *Fraser and McPherron*, 1982; *B. J. Anderson et al.*, 1992; *Fraser and Nguyen*, 2001]. The result in Figure 4 suggest that in the middle magnetosphere above ∼11° |MLat| EMIC waves do not undergo BWP propagation. Unidirectional propagation was found to be independent of wave frequency and wave band type suggesting that for the H+ branch waves there is no reflection from the bi-ion (f_{bi}) location off the equator. This result does not agree with the theoretical studies that found that these waves should be reflected from the bi-ion (f_{bi}) corresponding to around 10°–20° |MLat| [*Rauch and Roux*, 1982; *Perraut et al.*, 1984]. The results do agree with the experimental results of *Fraser et al.* [1996] using CRRES data and with a more recent study by *Mursula et al.* [2001] using conjugate data from the Polar spacecraft and the Finnish ground magnetometer stations. However, the Poynting vector results above 11° |MLat| presented here represent a more extensive data set and Mursula et al. estimated the energy flux only for one event and the results from both Mursula et al. and Fraser et al. were presented only in the time domain with no frequency discrimination which does not easily show the effects of multi-ion species on EMIC wave energy propagation in the magnetosphere.

[32] The unidirectional energy propagation results for all events above 11° |MLat| suggests that waves in the He+ branch do not undergo BWP motion and return energy from the ionosphere. This result also suggests that the bidirectional propagation seen within ∼11° is not due to BWP since CRRES would have observed some of this equatorward bidirectional energy above 11° |MLat|, if BWP propagation was a reality. Below ∼11° |MLat| the EMIC wave energy propagation results agree with the observations by *Fraser et al.* [1996]. The results in Figure 4 for the events below ∼11° |MLat| also suggest that CRRES was within the EMIC instability source region [*Fraser et al.*, 1996] where the ambient background magnetic field and consequently the resonant energy for the wave-particle interactions are minimized [e.g., *Cornwall*, 1965]. Beyond the generation region the EMIC waves propagate field guided toward the ionosphere and therefore observations at higher magnetic latitudes by CRRES are likely to only see unidirectional propagating wave packets. For the EMIC wave events seen off the equator at |MLat| > 11°, it is suggested that observed wave packet train structures are not due to BWP propagation. They may be related to long-period ULF wave modulation [e.g., *Mursula et al.*, 1997, 2001] and this will be discussed with respect to frequency domain observations in a future paper.

[33] The wave energy propagation characteristics shown in this paper also agree with recent Poynting vector results presented by *Trakhtengerts et al.* [2004] of a VLF whistler wave event observed within 6° |MLat| by the Cluster spacecrafts. They showed that the direction of the whistler wave energy propagation was bidirectional across a magnetic latitudinal extent of 3° centered at about 1° MLat. Outside this region only unidirectional energy propagation away from the equatorial region was observed. The results were explained by *Trakhtengerts et al.* [2004] as due to whistler wave generation according to a backward wave oscillator (BWO) regime [*Trakhtengerts*, 1995]. The BWO mechanism is well known in electronics [e.g., *Shevchik and Trubetskov*, 1975] and is analogous to the magnetospheric cyclotron maser concept [e.g., *Trakhtengerts*, 1995] where positive feedback or wave growth is established through the interaction of ELF/VLF noise with an oppositely propagating electron beam. In the BWO regime the electron instability at the equatorial generation region leads to an isotropic local electron velocity distribution due to velocity diffusion. This results in a step-like electron velocity distribution where whistler wave amplitudes can resonate resulting in wave growth. The absolute instability is due to phase bunching of the step electrons, which produces a positive feedback between the whistler-mode wave and a hot-plasma mode supported by the energetic electron maser. Over time this sharp step moves to higher latitudes, expanding the generation region and allowing for higher-frequency whistler wave growth. A spacecraft inside this generation region will observe bidirectional wave energy propagation, while outside it would observe the waves transmitted through the step boundary and moving away from the equator. *Trakhtengerts et al.* [2004] simulated the whistler wave energy flux using a BWO regime with a step-like electron velocity distribution and their results showed excellent agreement with the Cluster spacecraft observations. Since its generally accepted that EMIC wave generation is due to an ion cyclotron instability process similar to ELF/VLF emission involving electron cyclotron instability [e.g.,

Cornwall, 1965; *Obayashi*, 1965; *Kennel and Petschek*, 1966; *Jacobs and Watanabe*, 1966], an ion cyclotron analogy of the BWO regime used for VLF waves may explain the results presented here. However, a magnetospheric ion cyclotron maser based on the BWO regime has not been theoretically developed. Furthermore, experimental evidence is required of a step-like ion velocity distribution in the equatorial source region.

5. Conclusion

[34] The results from this study supports the growing evidence that cast doubt on the validity of the long-standing BWP paradigm that describes the propagation of electromagnetic ion cyclotron waves generated in the magnetosphere with frequencies close to the ion cyclotron frequency. For the first time the Poynting vector for EMIC waves was presented in the dynamic spectral domain, permitting the study of simultaneous waves located in different frequency bands. Bidirectional wave energy, propagating both away and toward the equator, was seen only for events observed below 11° |MLat|. Above 11° |MLat|, unidirectional propagation with wave energy moving away from the equator was observed for all events. The observed wave energy flux propagation directions were independent of wave branch and could not be explain by the BWP model. Any alternative to the bouncing wave packet paradigm should satisfy the question of how to generate structured wave packet trains or pearl EMIC waves in a multi-ion plasma magnetosphere that maintains unidirectional wave energy propagation outside the source region but allows for bidirectional wave energy propagation inside this region. Future work will concentrate on answering this question.

[35] **Acknowledgments.** This work was carried out in the Cooperative Research Centre for Satellite Systems with financial support from the Commonwealth of Australia through the CRC program, and the University of Newcastle, Australia. Thanks are due to R. A. Anderson for providing the CRRES electron density data and H. J. Singer for providing the AFGL magnetometer data. We also thank F. W. Menk and P. Ponomarenko for their useful discussions. Finally, we thank the reviewers for suggested changes and comments made.

[36] Lou-Chuang Lee thanks Robert E. Erlandson and Kalevi Mursula for their assistance in evaluating this paper.

References

Allis, W. P., S. J. Buchsbaum, and A. Bers (1963), *Waves in Anisotropic Plasmas*, MIT Press, Cambridge, Mass.

Anderson, B. J., R. E. Erlandson, and L. J. Zanetti (1992), A statistical study of Pc 1-2 magnetic pulsations in the equatorial magnetosphere: 1. Equatorial occurrence distributions, *J. Geophys. Res.*, *97*, 3075.

Anderson, R. R., D. A. Gurnett, and D. L. Odem (1992), CRRES plasma wave experiment, *J. Spacecr. Rockets*, *29*, 570.

Bossen, M., R. L. McPherron, and C. T. Russell (1976), A statistical study of Pc 1-2 magnetic pulsations at synchronous orbit, *J. Geophys. Res.*, *81*, 6083.

Cornwall, J. M. (1965), Cyclotron instabilities and electromagnetic emission in the ultra low frequency and very low frequency ranges, *J. Geophys. Res.*, *70*, 61.

Criswell, D. R. (1969), Pc1 micropulsations activity and magnetospheric application of 0.2 and 5.0 Hz hydomagnetic waves, *J. Geophys. Res.*, *74*, 205.

Erlandson, R. E., L. J. Zanetti, T. A. Potemra, L. P. Block, and G. Homgren (1990), Viking magnetic and electric field observation of Pc 1 waves and high latitude, *J. Geophys. Res.*, *95*, 5941.

Erlandson, R. E., B. J. Anderson, and L. J. Zanetti (1992), Viking magnetic and electric field observation of Pc 1 waves: Pearl pulsations, *J. Geophys. Res.*, *97*, 14,823.

Fraser, B. J. (1985), Observations of ion cyclotron waves near synchronous orbit and on the ground, in *Space Plasma Simulations*, edited by M. Ashour-Abdalla and D. Dutton, p. 357, Springer, New York.

Fraser, B. J., and R. L. McPherron (1982), Pc 1-2 magnetic pulsation spectra and heavy ion effects at synchronous orbit: ATS 6 results, *J. Geophys. Res.*, *87*, 4560.

Fraser, B. J., and T. S. Nguyen (2001), Is the plasmapause a preferred source region of electromagnetic ion cyclotron waves in the magnetosphere?, *J. Atmos. Sol. Terr. Phys.*, *63*, 1225.

Fraser, B. J., J. C. Samson, R. L. McPherron, and C. T. Russell (1992), Electromagnetic ion cyclotron wave observed near the oxygen cyclotron frequency by ISEE-1 and 2, *J. Geophys. Res.*, *97*, 3063.

Fraser, B. J., H. J. Singer, W. J. Hughes, J. R. Wygant, R. R. Anderson, and Y. D. Hu (1996), CRRES poynting vector observations of electromagnetic ion cyclotron waves near the plasmapause, *J. Geophys. Res.*, *101*, 15,331.

Gail, W. B. (1990), Theory of electromagnetic cyclotron wave growth in a time-varying magnetoplasma, *J. Geophys. Res.*, *95*, 19,089.

Gendrin, R. (1975), Is the plasmapause a preferential region for proton precipitation?, *Ann. Geophys.*, *31*, 127.

Jacobs, J. A., and T. Watanabe (1964), Micropulsation whistlers, *J. Atmos. Terr. Phys.*, *26*, 825.

Jacobs, J. A., and T. Watanabe (1966), Amplification of hydromagnetic waves in the magnetosphere by a cyclotron instability process with applications to the theory of hydromagnetic whistlers, *J. Atmos. Terr. Phys.*, *28*, 235.

Kaye, S. M., and M. G. Kivelson (1979), Observations of Pc 1-2 waves in the outer magnetosphere, *J. Geophys. Res.*, *84*, 4267.

Kaye, S. M., M. G. Kivelson, and D. Southwood (1979), Evolution of ion cyclotron instability in the plasma convection systems of the magnetosphere, *J. Geophys. Res.*, *84*, 6397.

Kennel, C. F., and H. E. Petschek (1966), Limit of stability trapped particle fluxes, *J. Geophys. Res.*, *71*, 1.

Kivelson, M. G., and C. T. Russell (1996), *Introduction to Space Physics*, Cambridge Univ. Press, New York.

LaBelle, J., and R. A. Treumann (1992), Poynting vector measurments of electromagnetic ion cyclotron waves in the plasmasphere, *J. Geophys. Res.*, *97*, 13,789.

Lorrain, P., D. P. Corson, and F. Lorrain (1988), *Electromagnetic Fields and Waves*, 3rd ed., W. H. Freeman, New York.

Loto'aniu, T. M., C. L. Waters, B. J. Fraser, and J. C. Samson (1999), Plasma mass density in the plasmatrough: Comparison using ulf waves and CRRES, *Geophys. Res. Lett.*, *21*, 26.

Mauk, B., and R. McPherron (1980), An experimental test of the electromagnetic ion cyclotron instability within the earth's magnetosphere, *Phys. Fluid*, *23*, 2111.

Mursula, K., R. Rasinkangas, T. Bosinger, R. E. Erlandson, and P. A. Lindqvist (1997), Nonbouncing Pc 1 wave bursts, *J. Geophys. Res.*, *102*, 17,611.

Mursula, K., T. Bräysy, K. Niskalia, and C. T. Russell (2001), Pc 1 pearl revisited: Structured electromagnetic ion cyclotron waves on POLAR satellite and on ground, *J. Geophys. Res.*, *106*, 29,543.

Obayashi, T. (1965), Hydromagnetic whistlers, *J. Geophys. Res.*, *70*, 1069.

Olson, W. P., and K. A. Pfitzer (1974), A quantitative model of the magnetospheric magnetic field, *J. Geophys. Res.*, *79*, 3739.

Perraut, S. (1982), Wave-particle interactions in the ulf range: GEOS-1 and -2 results, *Planet. Space. Sci.*, *30*, 1219.

Perraut, S., R. Gendrin, A. Roux, and C. de Villedary (1984), Ion cyclotron waves: Direct comparison between ground-based and observations in the source region, *J. Geophys. Res.*, *89*, 195.

Rauch, J. L., and A. Roux (1982), Ray tracing of ulf waves in a multicomponent magnetospheric plasma: Consequences for the generation of ion cyclotron waves, *J. Geophys. Res.*, *87*, 8191.

Shevchik, V. N., and D. I. Trubetskov (1975), *Electronics of Backward-Wave Tubes*, Saratov Univ. Press, Saratov, Russia.

Singer, H. J., W. P. Sullivan, P. Anderson, F. Mozer, P. Harvey, J. Wygant, and W. McNeil (1992), Fluxgate magnetometer instrument on the CRRES, *J. Spacecr. Rockets*, *29*, 599–601.

Stix, T. H. (1992), *Waves in Plasmas*, Am. Inst. of Phys., New York.

Tepley, L. (1964), Low-latitude observations of fine-structured hydromagnetic emissions, *Geophys. Res.*, *69*, 2273.

Trakhtengerts, V. Y. (1995), Magnetospheric cyclotron maser: Backward wave oscillator generation regime, *J. Geophys. Res.*, *100*, 17,205.

Trakhtengerts, V. Y., A. G. Demekhov, E. E. Titova, B. V. Kozelov, O. Santolik, D. Gurnett, and M. Parrot (2004), Interpretation of CLUSTER data on chorus emissions using the backward wave oscillator model, *Phys. Plasmas*, *11*, 1345.

Tsyganenko, N. A. (1987), Global quantitative models of the geomagnetic field in the cislunar magnetosphere for different disturbance levels, *Planet. Space Sci.*, *35*, 1347.

Walker, A. D. M. (1993), *Plasma Waves in the Magnetosphere, Physics and Chemistry in Space*, vol. 24, Springer, New York.

Wygant, J., P. R. Harvey, D. Pankow, F. S. Mozer, N. Maynard, H. Singer, M. Smiddy, W. Sullivan, and P. Anderson (1992), The CRRES electric field/langmuir probe instrument, *J. Spacecr. Rockets*, *29*, 601.

Young, D. T., S. Perraut, A. Roux, C. de Villedary, R. Gendrin, A. Korth, G. Kremser, and D. Jones (1981), Wave-particle interactions near Ω_{He+} observed on GEOS 1 and 2, 1. propagation of ion cyclotron waves in He^+-rich plasma, *J. Geophys. Res.*, *86*, 6755.

B. J. Fraser and C. L. Waters, School of Mathematical and Physical Sciences, University of Newcastle, Newcastle, NSW, 2308, Australia. (brian.fraser@newcastle.edu.au; colin.waters@newcastle.edu.au)

T. M. Loto'aniu, Department of Physics, University of Alberta, Edmonton, Alberta, T6G 2J1, Canada. (lotoaniu@phys.ualberta.ca)